ACS APPLIED MATERIALS & INTERFACES

Research Article

www.acsami.org

Solvothermal Synthesis of ZnO Nanoparticles and Anti-Infection Application in Vivo

Xiangyang Bai, Linlin Li, Huiyu Liu, Longfei Tan, Tianlong Liu,* and Xianwei Meng*

Laboratory of Controllable Preparation and Application of Nanomaterials, Center for Micro/nanomaterials and Technology, Technical Institute of Physics and Chemistry, Chinese Academy of Sciences, Beijing 100190, P. R. China

Supporting Information

ABSTRACT: Zinc oxide nanoparticles (ZnONPs) have been widely studied as the bacteriostatic reagents. However, synthesis of small ZnO nanoparticles with good monodispersion and stability in aqueous solution is still a challenge. Anti-infection research of ZnONPs used as antibacterial agent in vivo is rare. In this paper, a novel, sustainable, and simple method to synthesize ZnO nanoparticles with good monodispersion in aqueous low-temperature conditions and with a small molecule agent is reported. Inhibition zone test and the minimum inhibitory concentration test were performed to examine the antibacterial activity of ZnONPs against bacteria *Staphylococcus aureus* and *Escherichia coli* in vitro. For further application in vivo, low cytotoxicity and low acute toxicity in mice of ZnO were demonstrated. Finally, 4 nm ZnONPs combined with poly(vinyl alcohol) gel was used as antibacterial agent in rodent elytritis model, and significant anti-infection effect was proven. In one word, the present research would shed new light on the designing of antibacterial materials like ZnO with promising application in disinfection.

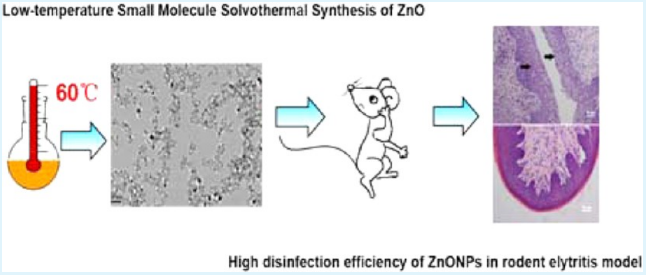

KEYWORDS: *ZnO nanoparticles, elytritis model, antibacterial activities, minimum inhibitory concentrations*

INTRODUCTION

The grand challenges of present antimicrobials involve the high incidence of bacterial infection in clinics and the growing of drug-resistant bacteria to conventional antibiotics all over the world.[1] Consequently, new agents and methods for bactericidal treatment of infections caused by bacteria are urgently needed. Nanomaterials have become increasingly used for biomedical applications and have shown great potential as a new drug to kill or inhibit numerous microorganisms.[2−6] Benefitting from the excellent antibacterial properties and low cytotoxicity, a few nanomaterials have been successfully applied in many fields including nanomedicines, antibacterial surfaces, wound dressing, protective clothing, food preservation, water treatment, and disinfecting agents.[7,8] However, the clinical application of NPs in disinfection is still rare. Most research has been focused on reducing the activity of microorganisms in vitro; nevertheless, animal models of infection are necessary to better understand the ability of nanomaterials to prevent or treat infection. Furthermore, the potential toxicity of nanomaterials aroused attention in recent years.[9−12] This means that more long-term, detailed toxicological studies of NPs are needed before clinical application.

Zinc oxide nanoparticles (ZnONPs) will act as a promising multifunctional material in the future. ZnONPs have a wide band gap with a large excitation binding energy (60 EV) and have an emission spectrum in the region of near-UV, which make it useful in solar cell applications, photocatalysis, and electronic sensor.[13−19] Furthermore, ZnONPs have shown antibacterial activity at very low concentration. And as antibacterial agent it has been successfully applied in some fields such as painting and cosmetics.[20−22] In the past decade, a variety of synthesis methods of ZnONPs with different morphologies have been reported, creating such moities as nanoparticles, nanorods,[23] nanotubes,[24] nanobelts,[25] nanoplates,[26] nanorings, and even nanoflowers.[27,28] The usual methods to synthesize ZnONPs include sol−gel,[29] hydrothermal,[30] mechanochemical,[31] vapor-phase method (VPM), coprecipitation,[32] and via solution.[33] These methods all have a common limitation that the product could not disperse well or rapid subsidence in water, and this prevents ZnONPs from being useful in biological fields.[34,35] Although surface modification can improve the dispersibility of ZnONPs in aqua, high-expensive surfactants increase the manufacture cost, including polyvinylpyrrolidone (PVP),[36] oleic acid (OA), together with diethanolamine (DEA),[37] polyethylene glycol methyl ether (PGME),[38] poly(methyl methacrylate) (PMMA),[39] and polystyrene (PS).[40] Synthesis of ZnONPs with good dispersibility in aqua by simple, green, and low-cost methods is still a challenge.

In recent decades, much research has reported on the antibacterial activity of ZnONPs. Some researchers have proved zinc oxide has antimicrobial activity in both microscale and

Received: October 29, 2014
Accepted: December 24, 2014
Published: December 24, 2014

DOI: 10.1021/am507532p
ACS Appl. Mater. Interfaces 2015, 7, 1308−1317

nanoscale formulations, and nanoscale particles are preferred in killing microorganisms.[41] Some researches investigate the minimum inhibitory concentration (MIC) of different sizes of ZnONPs against both Gram-negative and Gram-positive bacteria, and unique bactericidal mechanisms were discussed.[42,43] However, similar to other nanomaterials, most of them study the antibacterial activity of ZnONPs in vitro. For clinical biomedical applications, detailed information on anti-infection activity of ZnONPs in vivo is necessary. Furthermore, the systemic toxicity of ZnONPs in vitro and in vivo is not fully understood. The lack of research focused on antibacterial activity and toxicity of ZnONPs in vivo is the problem, which halts progression of nanomedicine based on ZnO nanoparticles.

In this manuscript, a simple method of synthesis ZnONPs with good dispersibility and different sizes in aqua is introduced. The optimized ZnONPs with powerful antibacterial activity were selected by inhibition zone test and the MIC test against bacteria *Staphylococcus aureus* and *Escherichia coli*. For the potential risk evaluation, cytotoxicity and acute toxicity of ZnONPs in vivo were examined when they exposed to mice after a single-dose intravenous injection and vaginal mucous membrane exposure for seven consecutive days, respectively. More importantly, to assess the antibacterial efficacy of ZnONPs in actual clinical disinfection, ZnONPs with poly(vinyl alcohol) (PVA) gel were prepared and showed excellent antibacterial property in mice elytritis (vaginitis) model caused by *E. coli* strains.

EXPERIMENTAL SECTION

Materials and Method. Zinc salt (0.015 M, Aldrich) and 0.1 g of dimethyl sulfone (Aldrich) were first dissolved in 80 mL of methanol reagent (Beijing Chemical Works) with continuous stirring at 60 °C. Subsequently, 40 mL of 0.001 M KOH (Aldrich) was added at the rate of 1 mL per minute, and the reaction was kept at 60 °C for 3 and 12 h to obtain the ZnO nanoparticles of 4 and 10 nm, respectively. The precipitate was washed three times with ethanol to remove soluble impurities, dried at 65 °C for 12 h, and stored at room temperature before use. Commercial ZnONP powder with size of 30 nm was purchased (Beijing Dk Nano technology Co., LTD) and used as control in this study.

Characterization of ZnO Nanoparticles. The crystal structure, size, morphology, and composition of the synthesized ZnO nanoparticles were investigated with powder X-ray diffraction (XRD), Fourier transform infrared spectroscopy (FTIR), field emission scanning electron microscopy (FESEM), transmission electron microscope (TEM), high-resolution transmission electron microscopy (HRTEM), and energy-dispersive spectrometry (EDS). Powder XRD was measured on Rigaku Ulima IV diffractometer operated at 40 kV and 44 mA using a Ni-filtered Cu Kα radiation with wavelength of 1.5408 Å in wide-angle region from 20° to 70° on 2θ scale. The data were analyzed with MDI Jade6 software. Infrared spectroscopy was performed on Excalibur 3100. The size, morphology, and composition were also performed by TEM (JEOL2100F) and EDS (Gatandatector) connecting to scanning electron microscope (S-4300).

Bacteria Growth. The Gram-negative bacteria *E. coli* (ATCC 25922) and Gram-positive bacteria *S. aureus* (ATCC 6538) were used to study the activities of ZnO nanoparticles antibacterial. β-Lactamase producing *E. coli* (CA-31) used in the experiment as drug resistant strain was isolated from the swine and gifted from College of Veterinary, China Agricultural University. All apparatus and materials were autoclaved and handled under sterile conditions during the experiments. *E. coli* and *S. aureus* were revived with Luria−Bertani (LB) broth and nutrient agar at 37 °C for 24 h. The density of bacterial cells in the liquid cultures was estimated by optical density (OD) measurements at 600 nm wavelength. The cell suspensions used for antibacterial activity contained 1×10^5 colony-forming units (CFU) mL^{-1}.

Agarose Diffusion Assay. The antimicrobial activity of ZnONPs was analyzed by agarose diffusion assay, and *E. coli*, *E. coli* (CA-31), and *S. aureus* were used as test organisms. The detailed information on the method can be found in ref 44. Briefly, the cell suspensions containing 1×10^5 colony-forming units (CFU) mL^{-1} were prepared. Then, 3 mL of cell suspensions were added into 100 mL of warmed (50 °C) agarose, poured into 15 mm square Petri dishes, and cooled to harden. Sample wells were made by punching holes with a 4 mm agar punch. A ZnONPs solution sample (20 μL) with different concentrations (labeled as 1−8 to indicate 1000, 500, 250, 200, 100, 50, 25, 12.5, and 0 μg/mL) was added to each well. Antimicrobial activity was quantitated by measuring the diameter of the circular clear zones on the opaque background of bacterial growth after incubation at 37 °C for 24 h.

Minimum Inhibitory Concentration Test. A sterile 96-well plate was used in MIC test. The modified resazurin method was used.[45] Briefly, a volume of 100 μL of test material in sterile water was pipetted into the 1−9 columns of the plate. Tips were discarded after use such that each well had 50 μL of the test material in serially descending concentrations. To the wells in columns 10−12 of the plate, 100 μL of nutrient broth or sterile saline was added. Serial dilutions were performed using a multichannel pipet. Finally, 10 μL of bacterial suspension (5×10^6 CFU/mL) was added to each well to achieve a concentration of 5×10^5 CFU/mL. Each plate had a set of controls: the 10 column with streptomycin as positive control, the 11 column with all solutions with the exception of the test compound as negative control, and the 12 column with all solutions with the exception of the bacterial solution adding 10 μL of nutrient broth instead as blank control. The plates were incubated at 37 °C for 18 h. Then 0.0675% resazurin solution was prepared, and a 10 μL aliquot was added to each well and incubated at 37 °C for 4 h. The color change was then assessed visually. Any color changes from purple to pink or colorless were recorded as positive. The lowest concentration at which color change occurred was taken as the MIC value. The average of three values was calculated, and that was the MIC for the test material and bacterial strain. The density of well was estimated by OD measurements at 570 nm wavelength, and the relative death rate of ZnONPs were calculated.

Cell Culture and Treatment. HepG-2 cells (human liver hepatocellular carcinoma cell line) and A-431 cells were maintained in high-glucose Dulbecco's modified Eagle's medium (DMEM), which was supplemented with 10% fetal bovine serum, 100 units/mL penicillin, and 100 μg/mL streptomycin at 37 °C in a humidified atmosphere of 5% CO_2. The cytotoxicity of ZnONPs was evaluated by 3-(4,5-dimethylthiazol-2-yl)-2,5-diphenyltetrazolium bromide (MTT) viability assay. After coincubating the cells with ZnONPs for 24 h at a series dosage, MTT solution was added to each well. After 4 h of incubation at 37 °C, colorimetric measurements were performed at 495 nm on a scanning multiwell spectrometer. Data were expressed as mean ± standard error of mean of at least five independent experiments.

Hemolysis Test. Hemolysis test was carried out using rabbit's heart blood to evaluate the cytotoxicity of the ZnONPs in vitro. Red blood cell solution (2%) was obtained after anticoagulation and washed with physiological saline solution three times. Then 1.2 mL cells were mixed with the 300 μL of ZnONPs diluted in physiological saline solution to obtain a series of final ZnONPs concentrations (25, 50, 100, 200, 500 μg/mL). The positive control group was the mixture of cells and the same volume of deionized water, and physiological saline solution was used as the negative control. Three parallel experiments were performed in duplicate for each group. The mixtures were centrifuged after placed at 37 °C for a 3 h incubation period. The absorbance of the supernatant was measured at 570 nm via UV−vis. The hemolysis ratio was calculated according to ratio of absorbance of ZnONPs groups divided by positive control subtracted from absorbance of negative control.

Animal and Treatments. Female ICR mice (provided by Vital River Laboratory Animal Technology Co. Ltd., Beijing), aged 6−8

DOI: 10.1021/am507532p
ACS Appl. Mater. Interfaces 2015, 7, 1308−1317

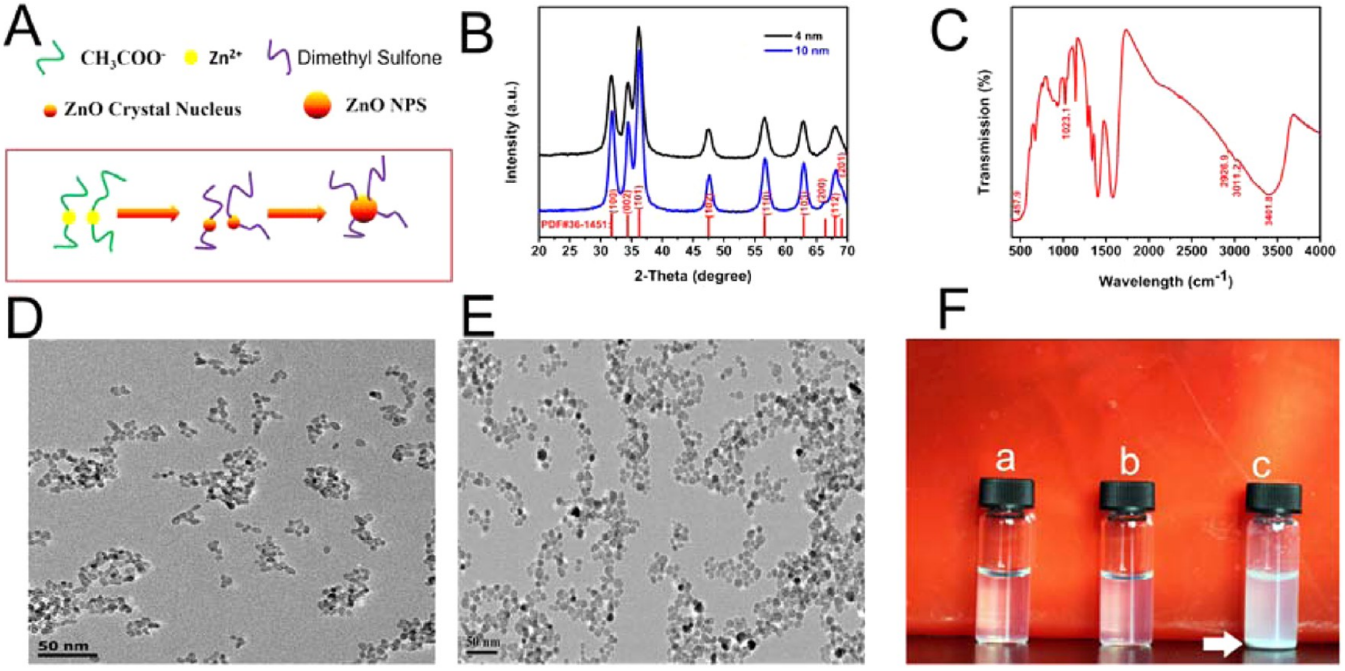

Figure 1. (A) Schematic diagram of ZnONPs preparation. (B) The XRD patterns of as-prepared ZnO nanoparticles with different sizes. (C) FTIR spectrum of ZnO nanoparticles with sample milled in KBr. D, E) TEM images of ZnO nanoparticles with different sizes 4 nm (D) and 10 nm (E). (F) Images of different sizes ZnONPs in water standing for 5 min after mixing. Four (a) and 10 nm (b) ZnONPs have good monodispersion in water. White arrow shows that commercial 30 nm ZnO (c) precipitate at the bottom of the bottle.

weeks, were used in the experiments. All animal experiments were conducted under protocols approved by the Laboratory Animal Centre of Peiking University, China. For acute toxicity, ICR mice received ZnONPs in 5% glucose by intravenous injection at different levels. Mice that received sterile 5% glucose by intravenous injections were used as controls. Five mice were used in each group. On day 14 after the injection, all the mice were sacrificed, and the serum and organs were recovered. The major organs were excised and performed for histological examination according to standard techniques. All the identity and analysis of the pathology slides were blind to the pathologist. For toxicity evaluation of ZnONPs when mice received them after vaginal mucous membrane exposure, mice received nanoparticles by vaginal douching with 50 μL of solution everyday for 7 d. On day 3 after the last douching, the mice were sacrificed, and the same treatments described above were repeated.

Serum Biochemical Analysis. Serum biochemical test was carried out using a standard protocol. After standing at room temperature for 4 h, the whole blood was centrifuged at 3000 rpm for 20 min. Then, serum was collected from the supernatant and examined by a biochemical autoanalyzer (Type 7170, Hitachi, Japan). Liver function was evaluated with serum levels of alanine aminotransferase (ALT) and aspartate aminotransferase (AST). Kidney function was evaluated with blood urea nitrogen (BUN) and creatinine (CREA).

Animal Anti-Infection Model Assay. Female ICR mice were anesthetized with isofluorane and inoculated vaginally with 5×10^6 CFU/mL *E. coli* in 50 μL of sterile phosphate-buffered saline for continuous 5 d. Clinical examination, vaginal washes, bacterial culture, and biochemical identification were performed to verify mice vaginitis model. Infected animals were divided into four groups including three treated groups and a control group (n = 6). ZnONPs solutions in water with different levels were mixed with PVA hydrogel and were inoculated vaginally to the animals. The final levels of ZnONPs in PVA hydrogel were 0.5, 1, and 2 mg/mL. All animals were treated continuously for 5 d and followed 3 d of recovery. On the last day, clinical examination, score of vaginosis, bacterial culture, and biochemical identification were performed. Colonies were evaluated and enumerated as recovered colony forming units (CFU) per milliliter of vaginal fluid. The vaginal tissue was collected for histological examination using standard techniques to assess the degree of inflammation. Epithelial thickness was measured with averages calculated from five measurements per vaginal section. Vaginal sections were collected and underwent Nugent scoring using published methods as previously described.[46]

Statistical Analysis. Results were expressed as mean ± standard deviation. Multigroup comparisons of the means were carried out by one-way analysis of variance test using SPSS 16.0 (SPSS Inc., Chicago, IL). The statistical significance for all tests was set at $p < 0.05$.

RESULT AND DISCUSSION

ZnONPs were formed through a solvothermal synthesis based on schematic diagram in Figure 1A. Briefly, zinc precursors were formed by the interaction of zinc acetate and dimethyl sulfone. Then, reacting with KOH, zinc precursors resulted in the formation of zinc oxide crystal nucleus. At last, ZnONPs were formed by the growth of zinc crystal nucleus. Because of the hydrophilic property of dimethyl sulfone, ZnONPs had a good dispersion in aqueous solution.

Figure 1B demonstrated typical XRD patterns of the as-prepared ZnO nanoparticles with different sizes (4 and 10 nm). The XRD patterns showed three strong peaks with d = 2.8143, 2.603, and 2.4759 Å. Three diffraction peaks could be indexed as the (100), (200), and (101) reflections with lattice constants of 3.346, 1.4072, and 5.205 Å, respectively. The synthesized ZnONPs had wurtzite structure. The other diffraction peaks in Figure 1 were consistent with JCPDS reference (PDF#36–1415). According to Scherrer formula, which was used in the determination of size of particles of crystals in the form of powder, the sizes of 4 and 10 nm ZnONPs were calculated by full width at half-maximum of (100) plane. At the same time, we found 10 nm ZnONPs had more acute peaks than the one with the size of 4 nm in Figure 1B. This suggested that 10 nm ZnONPs had better crystallinity and order of atomic arrangement in the crystal structure and that the lattice

DOI: 10.1021/am507532p
ACS Appl. Mater. Interfaces 2015, 7, 1308–1317

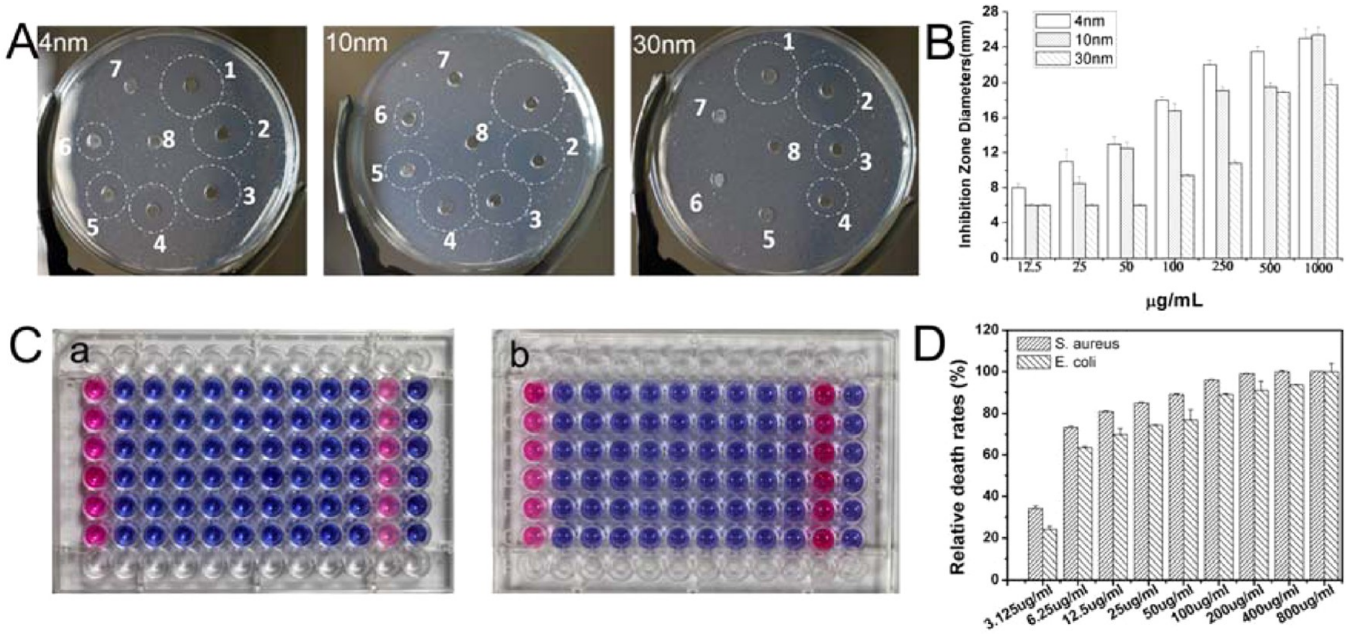

Figure 2. Results of inhibition zones tests and MIC tests of ZnONPs with different sizes and different concentrations. Four and 10 nm ZnONPs were prepared with the present method, 30 nm nanoparticles was commercial powder. (A) Images of inhibition zone of *E. coli* with different size ZnONPs incubation in 37 °C for 24 h. (B) Diameters of inhibition zone of ZnONPs against *E. coli* after incubation in 37 °C for 24 h. (C) Images of color variation of resazurin test of 4 nm ZnONPs against *E. coli* (a) and *S. aureus* (b) after incubation in 37 °C for 24 h. (D) Relative death rate of *E. coli* and *S. aureus* after incubation with 4 nm ZnONPs in 37 °C for 24 h.

matching degrees were more prefect than 4 nm ZnONPs. It maybe indirectly affects the antibacterial activity by tuning the gap of ZnO nanoparticles with various sizes.

Fourier transform infrared spectroscopy (FTIR) was applied to analysis of the surface structure of ZnO nanoparticles in Figure 1C recording in the 4000−400 cm^{-1} region. The band located at 457.9 cm^{-1} was assigned to the Zn−O stretching mode in the ZnO nanocrystals. The bands at 2926.9 and 3011.2 cm^{-1} were attributed to the absorbance band of methyl. The band at 3401.8 cm^{-1} was consistent with the absorbance band of −OH. The vibration band of S═O of dimethyl sulfone molecule was shifted from 1047 to 1023.1 cm^{-1}. It could be the result of a combination of zinc ion in the ZnO lattice with oxygen in the band of S═O in dimethyl sulfone. The ZnONPs observed by TEM are shown in Figure 1D,E. ZnONPs were almost spherical, and the nanoparticles were uniformly dispersed. TEM image revealed the average size of the as-prepared ZnONPs was ∼4 and 10 nm after 3 and 12 h of reaction, respectively. These values were in accordance with the results of XRD patterns. EDS connecting to FESEM was used to study the composition of ZnO nanoparticles. FESEM, EDS, and HRTEM results of 4 nm ZnONPs and 10 nm ZnONPs were shown in Supporting Information, Figure S1. The atomic ratio of zinc and oxygen was 1:1 from Figure S1, which proved the prepared particles were ZnO. Commercial ZnONPs of 30 nm were used in this study for comparing their antibacterial activates. TEM image of 30 nm ZnONPs was shown in Supporting Information, Figure S2. Compared with 4 and 10 nm ZnONPs, 30 nm ZnONPs have poor stability and dispersibility in water, and precipitation of 30 nm particles was quickly observed in water (Figure 1F).

Compared to the previous synthesis method, the preparation method has the following advantages. First, the presence of dimethyl sulfone benefits the good dispersion of ZnONPs in water. The unique sulfur−oxygen double bond structure of dimethyl sulfone may provide structural support as follows: First, one sulfur−oxygen bond could combine with ZnONPs by electrostatic force, and the other bond could improve the dispersity of ZnONPs in water. Second, the dimethyl sulfone is cheaper than long-chain ligands such as PVP, PMMA, PMMA, and PS reported in the literature. At the same time, dimethyl sulfone (named as methyl sulphonyl methane) is one necessary material of human collagen synthesis, which showed good biocompatibility.[47] The method was low-energy consumption, simple, and easy to scale-up for application in biological field in the future.

The Gram-negative bacteria *E. coli* (ATCC 25922), drug-resistant strain *E. coli* (CA-31), and Gram-positive bacteria *S. aureus* (ATCC 6538) were used as models for the investigation of the antibacterial activities of ZnONPs. Inhibition zones tests of ZnONPs with different sizes and different concentrations are shown in Figure 2. The results of the antibacterial properties of the prepared ZnO samples were compared with the commercial 30 nm ZnO powder. Inhibition zones tests could obtain visual observations results of reducing bacterial activity by measuring the area of the circular clear zones on the opaque background of bacterial growth. As shown in Figure 2A, number 1 to 6 wells of 4 and 10 nm size ZnONPs inhibition zone against *E. coli* were all clear. However, only 1 to 4 wells with 30 nm commercial ZnONPs had inhibition zones. The diameters of inhibition zone were measured with vernier caliper and exhibited in Figure 2B. The results of diameter of inhibition zone of ZnO against *S. aureus* were shown in Supporting Information, Figure S3. Compared to 30 nm ZnONPs, there was significant increase of antibacterial activity of 4 and 10 nm ZnO with concentration over 25 $\mu g\ mL^{-1}$. No difference was observed when ZnO concentration was 12.5 $\mu g/mL$. These results showed that ZnONPs prepared by the new methods have more enhanced antibacterial activity than that of commercial ZnO. According to different size particles, diameter

DOI: 10.1021/am507532p
ACS Appl. Mater. Interfaces 2015, 7, 1308−1317

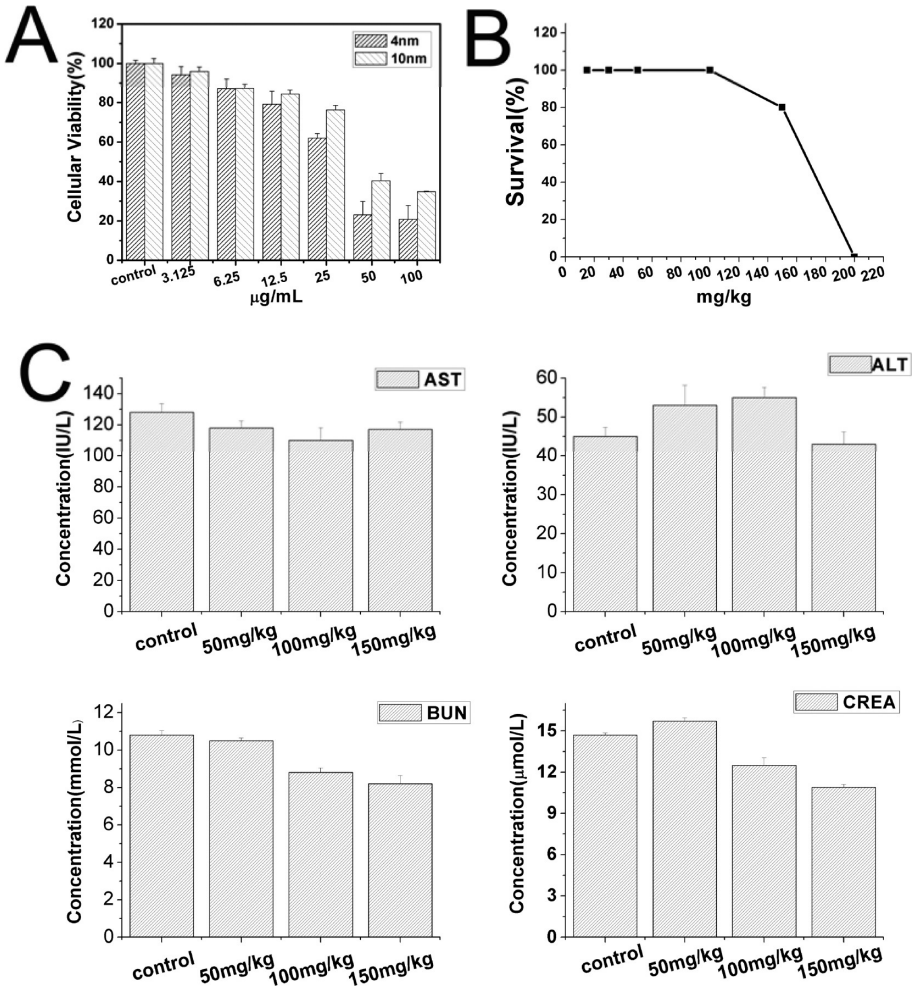

Figure 3. (A) Viability of cells exposed to 4 and 10 nm ZnONPs for 24 h. (B) Percentage of survival of mice that received ZnONPs suspension in 5% glucose solutions by intravenous injection (n = 5 per group). (C) Serum biochemical results of ICR mice following injection of ZnONPs. Mean and standard deviation of aspartate aminotransferase (AST), alanine aminotransferase (ALT), blood urea nitrogen (BUN), and creatinine (CREA) of ICR mice (n = 5 per group).

of inhibition zone of 4 nm ZnONPs was larger than that of 10 nm ZnONPs at level of 50 and 25 μg/mL (Figure 2B). For drug-resistant strain *E. coli* (CA-31), inhibition zones tests of ZnONPs with different sizes and concentrations were performed. As shown in Supporting Information, Figure S4, the 4 and 10 nm ZnONPs show greater inhibition than commercial 30 nm ZnO and control drug benzylpenicillin (a drug control). For β-lactamase producing *E. coli* (CA-31), benzylpenicillin can not inhibit the growth of the bacteria (Figure S4A–D). Compared with 30 nm ZnONPs, there was significant increase of antibacterial activity of 4 and 10 nm ZnO with concentration over 12.5 μg mL^{-1}. However, there was no significant difference between 4 and 10 nm ZnONPs against the drug-resistant strain.

For detailed quantitative evaluation of ZnO antibacterial effect, the MIC test was employed using 4 and 10 nm ZnO against bacteria *S. aureus* and *E. coli*. Figure 2C,D showed the MIC results of 4 nm ZnO against two experimental bacteria. In Figure 2C,a, the blue wells showing *E. coli* bacteria were inhibited by ZnO, and red wells meant the inhibition failed. The color change in Figure 2C,b showed the inhibition of *S. aureus* by 4 nm ZnONPs. The last blue wells not turned into red color indicated the MIC of ZnONPs. These results showed that MIC of 4 nm ZnO against both bacteria is 6.25 μg/mL. Relative inhibition rate of 4 nm ZnO upon bacteria is shown in Figure 2D. Inhibition rates of ZnO were over 60% in the presence of 6.25 μg/mL of 4 nm ZnO against two experimental bacteria. There was no significant difference between these two bacteria. The MIC results of 10 nm ZnO against *E. coli* and *S. aureus* were both 25 μg/mL (Supporting Information, Figure S5). These results indicated that 4 nm size particles had more powerful killing bacteria activity than 10 nm sized ZnONPs. The results also suggested concentration-dependent effect of ZnO against bacteria in vitro.

Antibacterial activities of ZnONPs have been extensively studied.[48] Some researches focus on distinction in the antibacterial activity depending on the shape, size, and the specific surface area of ZnO nanoparticles. Jiang et al. found nanoparticles had a more powerful antibacterial effect than microscale particles.[49] In recent years, antibacterial activity of ZnONPs with different sizes including 12, 13, 18, 40, 60 nm and lager scales were investigated against Gram-positive bacteria and Gram-negative bacteria. Padmavathy et al. reached the same conclusion that the bactericidal efficacy of ZnO nanoparticles increased with decreasing particle size.[50] Jones et al. showed 95% and 40%–50% inhibition of *S. aureus* growth in the presence of 1 mM 8 nm ZnO nanoparticles and 5 mM 50–70 nm ZnO after 10 h.[51] In the present study, the inhibition

DOI: 10.1021/am507532p
ACS Appl. Mater. Interfaces 2015, 7, 1308–1317

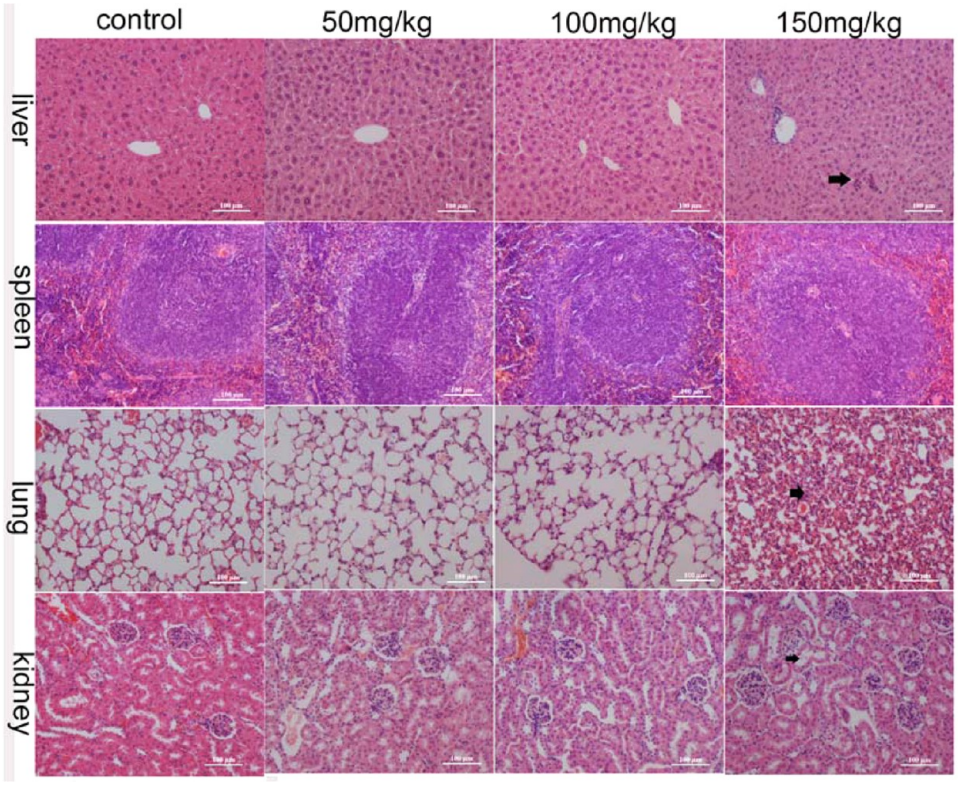

Figure 4. Histological analysis of tissues in control and ZnONPs-treated mice. ZnONPs were intravenously administered to mice at 0, 50, 100, and 150 mg/kg, respectively. Histological section of liver, spleen, lung, and kidney stained with H&E. Data are representative of at least five mice. ZnONPs induced damages in liver, lung, and kidney (arrowhead) at 150 mg/kg. The scale bar is 100 μm.

zone of commercial 30 nm ZnO disappeared when the concentration was less than 50 μg/mL; nevertheless, the dishes treated with prepared ZnONPs (4 and 10 nm) have a clear inhibition zone and diameters all greater than 10 mm even when the concentration was as low as 25 μg/mL. These results showed that ZnONPs prepared by the new present method was superior to commercial ZnO in antibacterial activity. Four nm and 10 nm size ZnONPs were used to kill Gram-positive and Gram-negative bacteria, and the MICs were 6.25 and 25 μg/mL, respectively. The activities of *E. coli* and *S. aureus* were reduced by 50% with 4 nm ZnO at 6.25 μg/mL and 10 nm ZnO at 25 μg/mL. These results agreed with previous researches conclusion that the antibacterial efficacy of ZnONPs increased with decreasing particle size. The detailed mechanism for the antibacterial activity of ZnO nanoparticles is still under debate. A main possible mechanism can be explained on the basis of the oxygen species released on the surface of ZnO, which causes fatal damage to microorganisms. When ZnO with defects is activated by UV or visible light, electron−hole pairs (e^-h^+) can be created. The holes split H_2O molecules into OH^- and H^+. Then dissolved oxygen molecules are transformed to superoxide radical anions and react with H^+ to generate ($HO_2^\bullet$) radicals, which upon subsequent collision with electrons produce hydrogen peroxide anions (HO_2^-). Hydrogen peroxide anions then react with hydrogen ions to produce molecules of H_2O_2. The production of H_2O_2 can penetrate the cell membrane and achieve bactericidal action. There are other theories including zinc ion release, mechanical damage of the cell membrane or cell wall, and the changes of the pH value caused by ZnO in the reaction system.[41] In a word, the bactericidal properties of ZnONPs are complicated and involve multifactorial antibacterial mechanisms.

The increased application of nanoparticles in many fields suggests that a full and fundamental understanding of their potential toxicity is needed. As with other NPs, the concerns for the risk caused by ZnONPs are being increased. Most studies reporting on ZnONPs toxicity have focused on mammalian cells, primarily on transformed cancer cell lines.[52] Diamond et al. reviewed the ecotoxicity of ZnONPs on bacteria and other microbes, algae and plants, invertebrates and vertebrate animals.[53] However, useful information about the toxicology of ZnONPs used in biomedical applications is missing, such as drug delivery or imaging, in which the NPs are deliberately placed in the body. Most of the toxicology studies of NPs in vivo so far were mainly concerned with the effects of NPs when they enter the body accidentally. Thorne et al. reported ZnONPs have low subchronic toxicity by the inhalation route.[54] Gao et al. researched the toxicity of 30 nm ZnONPs to the olfactory system when rat received NPs by intranasal instillation.[55] To the best of our knowledge, few in vivo studies exist on the toxicity of ZnONPs when they are deliberately placed in the body.[56]

The low cytotoxicity of NPs to human cells is the fundamental requirement for the use of ZnO nanopowders as antibacterial agents. For cytotoxicity study, HepG2 and A431 cell lines were used in the experiment. Viability of HepG2 cells exposed to ZnO for 24 h was all above 80% when concentrations are lower than 12.5 μg/mL. The IC_{50} of 4 and 10 nm ZnONPs was determinated as 28.16 and 36.25 μg/mL, respectively. According to A431 cells, the similar results were repeated. The IC_{50} of 4 and 10 nm ZnONPs to A431 cells were determinated as 25.45 and 38.34 μg/mL (Supporting Information, Figure S6B). Lower cytotoxicity of 10 nm ZnO than 4 nm ZnO was drawn from MTT results. The hemolysis

DOI: 10.1021/am507532p
ACS Appl. Mater. Interfaces 2015, 7, 1308−1317

ratio caused by 4 nm ZnONPs was evaluated as shown in Supporting Information, Figure S6A. None of the hemolysis ratio of all experimental groups exceeds 5%, and the maximum value was only 1.6%, indicating that ZnONPs showed good biocompatibility. Referring to the antibacterial and cytotoxicity results, 4 nm ZnONPs were chosen for further acute toxicity and disinfection in vivo.

The animal death caused by 4 nm ZnONPs is shown in Figure 3B when they entered blood circulation by intravenous injection. The mortality and clinical manifestation in each dose group was observed after exposure through the entire experiment. No death and unusual behaviors were observed in the low-dose groups (15, 30, 50, and 100 mg/kg), including vocalizations, labored breathing, difficulties in moving, hunching, or any unusual interactions with cage mates. But two mice, treated with ZnO at 200 mg/kg, died 30 min after injection, and one mouse died at 150 mg/kg dose (Figure 3B). No unusual weight changes of experiment groups were observed (Supporting Information, Figure S7). The lethal toxicity of 4 nm ZnO was lower than that of previous reports.[57]

For blood biochemical assay, AST, ALT, BUN, and CREA were examined. There was no significant change of serum levels of AST, BUN, and CREA of ZnO-treated groups compared with control animals (Figure 3C). A slight expansion with ALT at 100 mg/kg ZnO-treated animals was observed, but there was no significant difference compared with the control group. However, histopathological examinations revealed different results of ZnONPs toxicity with different concentrations. There were no unusual histological and morphological changes of main organs including liver, spleen, lung, and kidney of lower-dose (50 and 100 mg/kg) ZnO-treated groups. But mild inflammations were found in liver when mice received ZnONPs at 150 mg/kg dose. And thickened alveolar walls and inflammations happened in lung. Furthermore, renal tubular showed vacuolation degeneration gradually (Figure 4).

Because vaginitis models were used for examining the antibacterial activities, toxicity caused by ZnONPs was examined when mice received them after mucous membrane exposure. Six mice received 4 nm ZnONPs by vaginal mucous membrane exposure every day at 25 mg/kg for 7 d. No clinical manifestations were observed, including redness, swelling, itching of vagina, vocalizations, difficulties moving, hunching, or unusual interactions with cage mates. Figure 5 showed histopathological examinations results of major organs and vagina of experimental animals. No significant pathological changes were observed in liver, spleen, lung, kidney, and vagina when mice received ZnO by the exposure way as described above. All together, the lethality, serum biochemical index, and histopathological results indicated low acute toxicity of 4 nm ZnO when they entered the body by intravenous injection and mucous membrane exposure. These results provided a solid foundation for developing the novel ZnO-based biomaterials for disinfection in vivo.

The vaginitis models and therapeutic schedule was described in Figure 6A. Bacterial vaginitis (BV) mice models caused by *E. coli* were used in the experiment, and 4 nm ZnONPs dissolved in PVA polymer gel were prepared as disinfection agents for therapy. PVA polymer gel has many advantages including lubricity, biocompatibility, and flexibility. PVA polymer gel and relevant products have much promising application in biomedical areas such as bone repair, drug delivery, wound dressing, and ophthalmic products. In the present study, PVA polymer gel was used as effective carrier of ZnONPs. Vaginitis

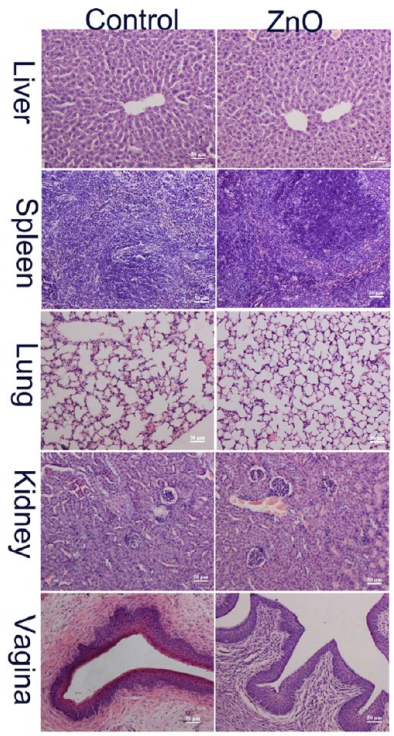

Figure 5. Histological analysis of tissues in ZnONPs-treated mice. Mice received ZnONPs by vaginal mucous membrane exposure at 25 mg/kg for 7 d. Histological section of liver, spleen, lung, kidney, and vagina stained with H&E. Data are representative of at least five mice. No significant changes were observed in liver, spleen, lung, kidney, and vagina when mice received ZnO. The scale bar is 50 μm.

mice received 50 μL of ZnONPs-PVA at three concentrations as 0.5, 1, and 2 mg/mL by vagina lavage every day for 5 d. The score of vaginitis was listed in Supporting Information, Table S1. At the last day, vaginal fluid was collected for bacterial counting. The animals were sacrificed, and samples of vagina were collected for histopathological examinations. As shown in Figure 6, compared with the healthy control animals (Figure 6B), the morphological changes of infection animals (Figure 6C) included desquamation and vanish of stratified squamous epithelium, inflammatory cell infiltration, and submucosa edema. Although these lesions existed in the low-dose ZnO group (0.5 mg/mL) (Figure 6D), edema and inflammatory cell infiltration did not happen in the high level (1 and 2 mg/mL) treated groups (Figure 6E). The results of bacterial counting (Supporting Information, Figure S8) and histological epithelial exfoliation score were consistent with the histopathological examinations. The mean CFU levels and exfoliation score in vaginal washes of both 1 and 2 mg/mL ZnO groups decreased significantly at the last day, suggesting clearance of the bacteria was occurring with ZnONPs. All these results indicated that ZnONPs could reduce the vagina inflammation caused by *E. coli*. BV was a common problem throughout the world as a kind of gynecological diseases. In the United States, one in three women has BV.[58] Women involved in BV disease were at high risk of pelvic inflammatory disease, infections, such as intrauterine infection and sexually transmitted infections, and preterm birth.[59] In the present study, mice vaginitis caused by *E. coli* was used as a model to verify the effectiveness of ZnONPs formulations in the treatment of vaginitis. This provides a feasible way to put ZnONPs into practical clinical application.

DOI: 10.1021/am507532p
ACS Appl. Mater. Interfaces 2015, 7, 1308−1317

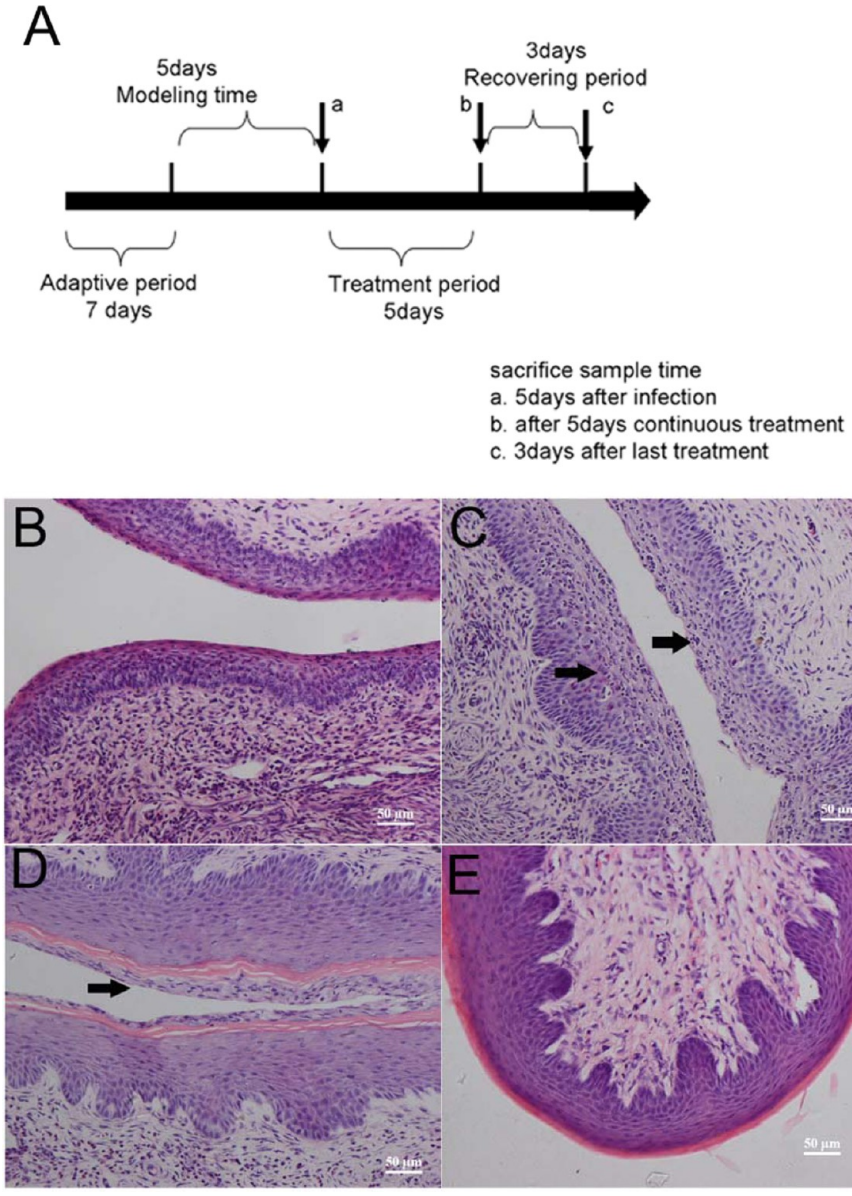

Figure 6. (A) Vaginitis models and therapeutic experimental design of ZnONPs in mice. (B) The morphological structure of the control animals' vagina. (C) The morphological changes of infection animals. Arrows indicate desquamation and vanish of stratified squamous epithelium. (D) Desquamation of epithelium cells in treated animals with low-level ZnONPs (0.5 mg/mL). Arrow indicates desquamation epithelium cells and inflammatory cells. (E) Desquamation of epithelium, edema, and inflammatory cell infiltration did not happen in the high-level groups (1 and 2 mg/mL). The scale bar is 50 μm.

CONCLUSION

In summary, hydrophilic ZnO nanoparticles with small sizes and good monodispersity were prepared by a simple, green, sustainable, and low-temperature solvothermal method, and the production showed excellent antibacterial properties at a low concentration. The cytotoxicity experiment and the acute toxicity in mice showed that the prepared ZnO had lower toxicity in vitro and in vivo. Pronounced therapeutic effect of vaginitis suggested a promising application of ZnONPs in biomedical fields. These results declared a promising biomedical application of ZnONPs in living animals. More detailed research and long-term toxicity studies are needed to confirm the injury caused by ZnONPs at high dosages. Further research of the antibacterial mechanism and the potential anti-infection effect of ZnONPs on the digestive tract and respiratory tract inflammation are needed, and these future studies will provide very useful information for future development of ZnO nanoparticles in biomedicine.

ASSOCIATED CONTENT

Supporting Information

SEM, FESEM, and HRTEM images and EDS results of ZnONPs, diameters of inhibition zone of ZnO against *S. Aureus,* MIC results, and the scores of vaginosis after treatment with ZnONPs. This material is available free of charge via the Internet at http://pubs.acs.org.

AUTHOR INFORMATION

Corresponding Authors

*Phone: (+86)10-82543521. Fax: (+86)10-82543521. E-mail: mengxw@mail.ipc.ac.cn. (X.M.)

*E-mail: tianlongipc@mail.ipc.ac.cn. (T.L.)

DOI: 10.1021/am507532p
ACS Appl. Mater. Interfaces 2015, 7, 1308−1317

Notes

The authors declare no competing financial interest.

■ ACKNOWLEDGMENTS

The authors acknowledge financial support from the National Natural Science Foundation of China (Project Nos. 81201814, 31270022, 81471784, 31271075, 51202260, and 61171049), National Hi-Tech Research and Development Program of China (Nos. 2013AA032201, 2012AA022701, and 2011AA02A114), and Beijing Nova Program (No. Z111103054511113).

■ REFERENCES

(1) Seil, J. T.; Webster, T. J. Antimicrobial Applications of Nanotechnology: Methods and Literature. *Int. J. Nanomed.* **2012**, *7*, 2767−2781.

(2) Davoudi, Z. M.; Kandjani, A. E.; Bhatt, A. I.; Kyratzis, I. L.; O'Mullane, A. P.; Bansal, V. Hybrid Antibacterial Fabrics with Extremely High Aspect Ratio Ag/AgTCNQ Nanowires. *Adv. Funct. Mater.* **2014**, *24*, 1047−1053.

(3) Alonso, A.; Munoz-Berbel, X.; Vigues, N.; Rodriguez-Rodriguez, R.; Macanas, J.; Munoz, M.; Mas, J.; Muraviev, D. N. Superparamagnetic Ag@Co-Nanocomposites on Granulated Cation Exchange Polymeric Matrices with Enhanced Antibacterial Activity for the Environmentally Safe Purification of Water. *Adv. Funct. Mater.* **2013**, *23*, 2450−2458.

(4) Bindhu, M. R.; Umadevi, M. Silver and Gold Nanoparticles for Sensor and Antibacterial Applications. *Spectrochim. Acta, Part A* **2014**, *128*, 37−45.

(5) Li, Y.; Zhang, W.; Niu, J. F.; Chen, Y. S. Mechanism of Photogenerated Reactive Oxygen Species and Correlation with the Antibacterial Properties of Engineered Metal-Oxide Nanoparticles. *ACS Nano* **2012**, *6*, 5164−5173.

(6) Li, L. L.; Wang, H. Enzyme-Coated Mesoporous Silica Nanoparticles as Efficient Antibacterial Agents in Vivo. *Adv. Healthcare Mater.* **2013**, *2*, 1351−1360.

(7) Sun, H. J.; Gao, N.; Dong, K.; Ren, J. S.; Qu, X. G. Graphene Quantum Dots-Band-Aids Used for Wound Disinfection. *ACS Nano* **2014**, *8*, 6202−6210.

(8) Lin, Z. H.; Cheng, G.; Wu, W. Z.; Pradel, K. C.; Wang, Z. L. Dual-Mode Triboelectric Nanogenerator for Harvesting Water Energy and as a Self-Powered Ethanol Nanosensor. *ACS Nano* **2014**, *8*, 6440−6448.

(9) Winnik, F. M.; Maysinger, D. Quantum Dot Cytotoxicity and Ways To Reduce It. *Acc. Chem. Res.* **2013**, *46*, 672−680.

(10) Ji, Z.; Wang, X.; Zhang, H.; Lin, S.; Meng, H.; Sun, B.; George, S.; Xia, T.; Nel, A. E.; Zink, J. I. Designed Synthesis of CeO_2 Nanorods and Nanowires for Studying Toxicological Effects of High Aspect Ratio Nanomaterials. *ACS Nano* **2012**, *6*, 5366−5380.

(11) Zhang, Y. B.; Xu, Y.; Li, Z. G.; Chen, T.; Lantz, S. M.; Howard, P. C.; Paule, M. G.; Slikker, W.; Watanabe, F.; Mustafa, T.; Biris, A. S.; Ali, S. F. Mechanistic Toxicity Evaluation of Uncoated and PEGylated Single-Walled Carbon Nanotubes in Neuronal PC12 Cells. *ACS Nano* **2011**, *5*, 7020−7033.

(12) Jeong, Y. S.; Oh, W. K.; Kim, S.; Jang, J. Cellular Uptake, Cytotoxicity, and ROS Generation with Silica/conducting Polymer Core/shell Nanospheres. *Biomaterials* **2011**, *32*, 7217−7225.

(13) Ozgur, U.; Alivov, Y. I.; Liu, C.; Teke, A.; Reshchikov, M. A.; Dogan, S.; Avrutin, V.; Cho, S. J.; Morkoc, H. A Comprehensive Review of ZnO Materials and Devices. *J. Appl. Physiol.* **2005**, *98*, 041301−041404.

(14) Jeong, W. J.; Kim, S. K.; Park, G. C. Preparation and Characteristic of ZnO Thin Film with High and Low Resistivity for an Application of Solar Cell. *Thin Solid Films* **2006**, *506*, 180−183.

(15) Look, D. C. Recent Advances in ZnO Materials and Devices. *Mater. Sci. Eng., B* **2001**, *80*, 383−387.

(16) Moritz, M.; Geszke-Moritz, M. The Newest Achievements in Synthesis, Immobilization and Practical Applications of Antibacterial Nanoparticles. *Chem. Eng. J.* **2013**, *228*, 596−613.

(17) Nair, M. G.; Nirmala, M.; Rekha, K.; Anukaliani, A. Structural, Optical, Photo Catalytic and Antibacterial Activity of ZnO and Co doped ZnO Nanoparticles. *Mater. Lett.* **2011**, *65*, 1797−1800.

(18) Sun, X.; Maeda, K.; Le Faucheur, M.; Teramura, K.; Domen, K. Preparation of $(Ga_{(1-x)}Zn_x)$ $(N_{(1-x)}O_x)$ Solid-solution from $ZnGa_2O_4$ and ZnO as a Photo-catalyst for Overall Water Splitting under Visible Light. *Appl. Catal., A* **2007**, *327*, 114−121.

(19) Wan, Q.; Li, Q. H.; Chen, Y. J.; Wang, T. H.; He, X. L.; Li, J. P.; Lin, C. L. Fabrication and Ethanol Sensing Characteristics of ZnO Nanowire Gas Sensors. *Appl. Phys. Lett.* **2004**, *84*, 3654−3656.

(20) Sawai, J. Quantitative Evaluation of Antibacterial Activities of Metallic Oxide Powders (ZnO, MgO and CaO) by Conductimetric Assay. *J. Microbiol. Methods* **2003**, *54*, 177−182.

(21) Sun, Q.; Tran, M.; Smith, B.; Winefordner, J. D. In-situ Evaluation of Barrier-cream Performance on Human Skin Using Laser-induced Breakdown Spectroscopy. *Contact Dermatitis* **2000**, *43*, 259−263.

(22) Ghule, K.; Ghule, A. V.; Chen, B. J.; Ling, Y. C. Preparation and Characterization of ZnO Nanoparticles Coated Paper and its Antibacterial Activity Study. *Green Chem.* **2006**, *8*, 1034−1041.

(23) Liu, B.; Zeng, H. C. Hydrothermal Synthesis of ZnO Nanorods in the Diameter Regime of 50 nm. *J. Am. Chem. Soc.* **2003**, *125*, 4430−4431.

(24) Sun, Y.; Fuge, G. M.; Fox, N. A.; Riley, D. J.; Ashfold, M. N. R. Synthesis of Aligned Arrays of Ultrathin ZnO Nanotubes on a Si Wafer Coated with a Thin ZnO Film. *Adv. Mater.* **2005**, *17*, 2477−2481.

(25) Wang, W. Z.; Zeng, B. Q.; Yang, J.; Poudel, B.; Huang, J. Y.; Naughton, M. J.; Ren, Z. F. Aligned Ultralong ZnO Nanobelts and Their Enhanced Field Emission. *Adv. Mater.* **2006**, *18*, 3275−3278.

(26) Huang, J. R.; Wu, Y. J.; Gu, C. P.; Zhai, M. H.; Sun, Y. F.; Liu, J. H. Fabrication and Gas-sensing Properties of Hierarchically Porous ZnO Architectures. *Sens. Actuators, B* **2011**, *155*, 126−133.

(27) Hughes, W. L.; Wang, Z. L. Controlled Synthesis and Manipulation of ZnO Nanorings and Nanobows. *Appl. Phys. Lett.* **2005**, *86*, 041306.

(28) Wahab, R.; Ansari, S. G.; Kim, Y. S.; Seo, H. K.; Kim, G. S.; Khang, G.; Shin, H. S. Low Temperature Solution Synthesis and Characterization of ZnO Nano-flowers. *Mater. Res. Bull.* **2007**, *42*, 1640−1648.

(29) Joo, J.; Kwon, S. G.; Yu, J. H.; Hyeon, T. Synthesis of ZnO Nanocrystals with Cone, Hexagonal Cone, and Rod Shapes via Non-Hydrolytic Ester Elimination Sol−Gel Reactions. *Adv. Mater.* **2005**, *17*, 1873−1877.

(30) Cheng, B.; Samulski, E. T. Hydrothermal Synthesis of One-dimensional ZnO Nanostructures with Different Aspect Ratios. *Chem. Commun.* **2004**, 986−987.

(31) Banoee, M.; Seif, S.; Nazari, Z. E.; Jafari-Fesharaki, P.; Shahverdi, H. R.; Moballegh, A.; Moghaddam, K. M.; Shahverdi, A. R. ZnO Nanoparticles Enhanced Antibacterial Activity of Ciprofloxacin Against Staphylococcus Aureus and Escherichia Coli. *J. Biomed. Mater. Res., Part B* **2010**, *93B*, 557−561.

(32) Kripal, R.; Gupta, A. K.; Srivastava, R. K.; Mishra, S. K. Photoconductivity and Photoluminescence of ZnO Nanoparticles Synthesized via Co-precipitation Method. *Spectrochim. Acta, Part A* **2011**, *79*, 1605−1612.

(33) Wahab, R.; Hwang, I. H.; Kim, Y.-S.; Shin, H.-S. Photocatalytic Activity of Zinc Oxide Micro-flowers Synthesized Via Solution Method. *Chem. Eng. J.* **2011**, *168*, 359−366.

(34) Xiong, H. M. Photoluminescent ZnO Nanoparticles Modified by Polymers. *J. Mater. Chem.* **2010**, *20*, 4251−4262.

(35) Xiong, H. M. ZnO Nanoparticles Applied to Bioimaging and Drug Delivery. *Adv. Mater.* **2013**, *25*, 5329−5335.

(36) Guo, L.; Yang, S. H.; Yang, C. L.; Yu, P.; Wang, J. N.; Ge, W. K.; Wong, G. K. L. Synthesis and Characterization of Poly-

DOI: 10.1021/am507532p
ACS Appl. Mater. Interfaces 2015, 7, 1308−1317

(vinylpyrrolidone)-modified Zinc Oxide Nanoparticles. *Chem. Mater.* **2000**, *12*, 2268−2274.
(37) Fu, Y. S.; Du, X. W.; Kulinich, S. A.; Qiu, J. S.; Qin, W. J.; Li, R.; Sun, J.; Liu, J. Stable Aqueous Dispersion of ZnO Quantum Dots with Strong Blue Emission Via Simple Solution Route. *J. Am. Chem. Soc.* **2007**, *129*, 16029−16033.
(38) Xiong, H. M.; Wang, Z. D.; Liu, D. P.; Chen, J. S.; Wang, Y. G.; Xia, Y. Y. Bonding Polyether onto ZnO Nanoparticles: An Effective Method for Preparing Polymer Nanocomposites with Tunable Luminescence and Stable Conductivity. *Adv. Funct. Mater.* **2005**, *15*, 1751−1756.
(39) Xiong, H. M.; Wang, Z. D.; Xia, Y. Y. Polymerization Initiated by Inherent Free Radicals on Nanoparticle Surfaces: A Simple Method of Obtaining Ultrastable (ZnO)polymer Core-shell Nanoparticles with Strong Blue Fluorescence. *Adv. Mater.* **2006**, *18*, 748−751.
(40) Xiong, H. M.; Xie, D. P.; Guan, X. Y.; Tan, Y. J.; Xia, Y. Y. Water-stable Blue-emitting ZnO@polymer Core-shell Microspheres. *J. Mater. Chem.* **2007**, *17*, 2490−2496.
(41) Stankovic, A.; Dimitrijevic, S.; Uskokovic, D. Influence of Size Scale and Morphology on Antibacterial Properties of ZnO Powders Hydrothemally Synthesized Using Different Surface Stabilizing Agents. *Colloids Surf., B* **2013**, *102*, 21−28.
(42) Matai, I.; Sachdev, A.; Dubey, P.; Kumar, S. U.; Bhushan, B.; Gopinath, P. Antibacterial Activity and Mechanism of Ag-ZnO Nanocomposite on S. aureus and GFP-expressing Antibiotic Resistant E-coli. *Colloids Surf., B* **2014**, *115*, 359−367.
(43) Dutta, R. K.; Nenavathu, B. P.; Gangishetty, M. K.; Reddy, A. V. R. Antibacterial Effect of Chronic Exposure of Low Concentration ZnO Nanoparticles on E. coli. *J. Environ. Sci. Health, Part A: Environ. Sci. Eng.* **2013**, *48*, 871−878.
(44) Lehrer, R. I.; Rosenman, M.; Harwig, S. S. S. L.; Jackson, R.; Eisenhauer, P. Ultrasensitive Assays for Endogenous Antimicrobial Polypeptides. *J. Immunol. Methods* **1991**, *137*, 167−173.
(45) Elavarasan, T.; Chhina, S. K.; Parameswaran, M.; Sankaran, K. Resazurin Reduction Based Colorimetric Antibiogram in Microfluidic Plastic Chip. *Sens. Actuators, B* **2013**, *176*, 174−180.
(46) Lewis, W. G.; Robinson, L. S.; Perry, J.; Bick, J. L.; Peipert, J. F.; Allsworth, J. E.; Lewis, A. L. Hydrolysis of Secreted Sialoglycoprotein Immunoglobulin A (IgA) in ex Vivo and Biochemical Models of Bacterial Vaginosis. *J. Biol. Chem.* **2012**, *287*, 2079−2089.
(47) Maranon, G.; Munoz-Escassi, B.; Manley, W.; Garcia, C.; Cayado, P.; de la Muela, M. S.; Olabarri, B.; Leon, R.; Vara, E. The Effect of Methyl Sulphonyl Methane Supplementation on Biomarkers of Oxidative Stress in Sport Horses Following Jumping Exercise. *Acta Vet. Scand.* **2008**, *50*, 45.
(48) Ng, Y. H.; Leung, Y. H.; Liu, F. Z.; Ng, A. M. C.; Gao, M. H.; Chan, C. M. N.; Djurisic, A. B.; Leung, F. C. C.; Chan, W. K. Antibacterial Activity of ZnO Nanoparticles Under Ambient Illumination - The Effect of Nanoparticle Properties. *Thin Solid Films* **2013**, *542*, 368−372.
(49) Jiang, W.; Mashayekhi, H.; Xing, B. S. Bacterial Toxicity Comparison Between Nano- and Micro-scaled Oxide Particles. *Environ. Pollut.* **2009**, *157*, 1619−1625.
(50) Padmavathy, N.; Vijayaraghavan, R. Enhanced Bioactivity of ZnO Nanoparticles-an Antimicrobial Study. *Sci. Technol. Adv. Mater.* **2008**, *9*, 035004.
(51) Jones, N.; Ray, B.; Ranjit, K. T.; Manna, A. C. Antibacterial Activity of ZnO Nanoparticle Suspensions on a Broad Spectrum of Microorganisms. *FEMS Microbiol. Lett.* **2008**, *279*, 71−76.
(52) Reddy, K. M.; Feris, K.; Bell, J.; Wingett, D. G.; Hanley, C.; Punnoose, A. Selective Toxicity of Zinc Oxide Nanoparticles to Prokaryotic and Eukaryotic systems. *Appl. Phys. Lett.* **2007**, *90*, 213902.
(53) Ma, H. B.; Williams, P. L.; Diamond, S. A. Ecotoxicity of Manufactured ZnO Nanoparticles - A Review. *Environ. Pollut.* **2013**, *172*, 76−85.
(54) Adamcakova-Dodd, A.; Stebounova, L. V.; Kim, J. S.; Vorrink, S. U.; Ault, A. P.; O'Shaughnessy, P. T.; Grassian, V. H.; Thorne, P. S. Toxicity Assessment of Zinc Oxide Nanoparticles Using Sub-acute and Sub-chronic Murine Inhalation Models. *Part. Fibre Toxicol.* **2014**, *11*, 15−30.
(55) Gao, L. F.; Yang, S. T.; Li, S. R.; Meng, Y. G.; Wang, H. F.; Lei, H. Acute Toxicity of Zinc Oxide Nanoparticles to the Rat Olfactory System after Intranasal Instillation. *J. Appl. Toxicol.* **2013**, *33*, 1079−1088.
(56) Chen, J. K.; Shih, M. H.; Peir, J. J.; Liu, C. H.; Chou, F. I.; Lai, W. H.; Chang, L. W.; Lin, P. P.; Wang, M. Y.; Yang, M. H.; Yang, C. S. The Use of Radioactive Zinc Oxide Nanoparticles in Determination of Their Tissue Concentrations Following Intravenous Administration in Mice. *Analyst* **2010**, *135*, 1742−1746.
(57) Esmaeillou, M.; Moharamnejad, M.; Hsankhani, R.; Tehrani, A. A.; Maadi, H. Toxicity of ZnO Nanoparticles in Healthy Adult Mice. *Environ. Toxicol. Pharmacol.* **2013**, *35*, 67−71.
(58) Gilbert, N. M.; Lewis, W. G.; Lewis, A. L. Clinical Features of Bacterial Vaginosis in a Murine Model of Vaginal Infection with Gardnerella vaginalis. *PLoS One* **2013**, *8*, e59539.
(59) Martins, G.; Figueira, L.; Penna, B.; Brandao, F.; Varges, R.; Vasconcelos, C.; Lilenbaum, W. Prevalence and Antimicrobial Susceptibility of Vaginal Bacteria from Ewes Treated with Progestin-impregnated Intravaginal Sponges. *Small Ruminant Res.* **2009**, *81*, 182−184.

DOI: 10.1021/am507532p
ACS Appl. Mater. Interfaces 2015, 7, 1308−1317